Materials Today Bio 25 (2024) 100958

Contents lists available at ScienceDirect

Materials Today Bio

journal homepage: www.journals.elsevier.com/materials-today-bio

Mi-BMSCs alleviate inflammation and fibrosis in CCl_4-and TAA-induced liver cirrhosis by inhibiting TGF-β/Smad signaling

Qing Shi [a,1], Yuhan Xia [a,1], Minmin Wu [a,1], Yating Pan [a], Shiyi Wu [a], Jiawei Lin [a], Yifan Kong [a], Zhijie Yu [b], Xingjie Zan [c,*], Pixu Liu [a,**], Jinglin Xia [a,d,e,***]

[a] Key Laboratory of Diagnosis and Treatment of Severe Hepato-Pancreatic Diseases of Zhejiang Province, The First Affiliated Hospital of Wenzhou Medical University, Wenzhou, 325000, Zhejiang, China
[b] Wenzhou Key Laboratory of Hematology, The First Affiliated Hospital of Wenzhou Medical University, Wenzhou, 325000, Zhejiang, China
[c] Wenzhou Institute, Wenzhou Key Laboratory of Perioperative Medicine, University of Chinese Academy of Sciences, Wenzhou, 325001, China
[d] Liver Cancer Institute, Zhongshan Hospital of Fudan University, Shanghai, 200032, China
[e] National Clinical Research Center for Interventional Medicine, Shanghai, 200032, China

ARTICLE INFO

Keywords:
Porous microspheres
Bone marrow mesenchymal stem cells
Liver cirrhosis
Fibrosis
TGF-β/Smad

ABSTRACT

Cirrhosis is an aggressive disease, and over 80 % of liver cancer patients are complicated by cirrhosis, which lacks effective therapies. Transplantation of mesenchymal stem cells (MSCs) is a promising option for treating liver cirrhosis. However, this therapeutic approach is often challenged by the low homing ability and short survival time of transplanted MSCs *in vivo*. Therefore, a novel and efficient cell delivery system for MSCs is urgently required. This new system can effectively extend the persistence and duration of MSCs *in vivo*. In this study, we present novel porous microspheres with microfluidic electrospray technology for the encapsulation of bone marrow-derived MSCs (BMSCs) in the treatment of liver cirrhosis. Porous microspheres loaded with BMSCs (Mi-BMSCs) exhibit good biocompatibility and demonstrate better anti-inflammatory properties than BMSCs alone. Mi-BMSCs significantly increase the duration of BMSCs and exert potent anti-inflammatory and anti-fibrosis effects against CCl_4 and TAA-induced liver cirrhosis by targeting the TGF-β/Smad signaling pathway to ameliorate cirrhosis, which highlight the potential of Mi-BMSCs as a promising therapeutic approach for early liver cirrhosis.

1. Introduction

Liver cirrhosis is a malignant disease characterized by progressive liver fibrosis, pseudolobular formation, and hyperplasia of intrahepatic and extrahepatic blood vessels. It seriously damages the structure and function of the liver and causes approximately 2 million deaths per year [1]. At the early stage of liver cirrhosis, hepatic stellate cells (HSCs) become activated under chronic inflammatory stimulation (such as viral hepatitis and non-alcoholic steatohepatitis) [2]. These activated HSCs transform into myofibroblasts, which produce a large amount of extracellular matrix (ECM), playing a crucial role in the formation of liver fibrosis [3]. Under the constant irritation of chronic inflammation, persistent liver fibrosis can develop into irreversible advanced cirrhosis and further progress to hepatocellular carcinoma, leading to potentially fatal complications. There is increasing evidence that preventing the activation of HSCs and disrupting the biological chain of liver fibrosis at an early stage is crucial for impeding or reversing the progression of liver cirrhosis [3–5]. However, due to the lack of effective anti-fibrosis methods or drugs, current clinical treatments can only manage the symptoms of patients with decompensated cirrhosis, without the ability to reverse or impede the progression of liver fibrosis [6,7]. Therefore, the pursuit of advanced therapeutic strategies to impede or reverse the progress of liver cirrhosis remain crucial.

Mesenchymal stem cells (MSCs) derived from bone marrow have

* Corresponding author.
** Corresponding author.
*** Corresponding author. Key Laboratory of Diagnosis and Treatment of Severe Hepato-Pancreatic Diseases of Zhejiang Province, The First Affiliated Hospital of Wenzhou Medical University, Wenzhou 325000, Zhejiang, China.
E-mail addresses: zanxj@ucas.ac.cn (X. Zan), pixuliu@wmu.edu.cn (P. Liu), xiajinglin@fudan.edu.cn (J. Xia).
[1] **Note:** They contributed equally to this work.

https://doi.org/10.1016/j.mtbio.2024.100958
Received 16 October 2023; Received in revised form 8 January 2024; Accepted 15 January 2024
Available online 24 January 2024

garnered considerable attention across various disciplines due to their remarkable self-replication, renewal, and differentiation capabilities into a variety of desired cell types [8]. Moreover, their low intrinsic immunogenicity makes MSCs highly suitable for transplantation to treat various diseases [9], including acute and chronic liver diseases, anti-aging, cardiomyopathy, immune system diseases, metabolic syndrome, Alzheimer's disease, novel coronaviruses, and tumors [10–12]. Extensive evidence has demonstrated that MSC-based therapy for liver cirrhosis primarily targets anti-inflammatory and anti-fibrotic effects, as well as promoting liver repair through paracrine cytokines, immune regulation, and facilitation of extracellular matrix degradation via various signaling pathways, such as TGF-β1/SMAD, Wnt/β-catenin, Ras/ERK, or Notch [13–18]. Presently, the transplantation of MSCs for the treatment of liver cirrhosis has been registered and its therapeutic effect has been verified in numerous clinical trials [19–21]. However, the main method of MSCs transplantation, peripheral intravenous injection, results in approximately 80 % of MSCs being distributed in the lungs. This quick recognition and elimination by the immune system, along with the difficulty of enriching MSCs in target organs, leads to shortened retention *in vivo* and greatly limits their therapeutic effectiveness [22,23]. Therefore, there is an urgent need for new delivery technologies, such as cell carriers and modified cells, to reduce elimination, prolong *in vivo* retention, and enhance organ targeting.

Hydrogel, a crosslinked hydrophilic polymer with a 3-dimensional structure that can absorb a considerable amount of water, has found extensive applications in tissue engineering and cellular delivery. The porous nature of hydrogel enables cell entrapment, facilitates nutrient exchange, and promotes metabolic excretion [24]. Due to its high safety profile and cost-effectiveness, hydrogel microspheres have emerged as highly promising platforms for cell delivery systems. The hydrogel porous microspheres can protect BMSCs from immune cell recognition and prolong the long-term function and cytokine release *in vivo*, which is beneficial to the long-term survival and the curative effect of MSCs. Levit et al. [25]. proposed a biocompatible polyethylene glycol (PEG) hydrogel patch with alginate encapsulated MSCs for intramyocardial delivery of MSC, which significantly improved cardiac function, reduced the range of myocardial infarction and increased microvessel density. However, these common block hydrogels are not convenient for direct injection, and cannot realize rapid exchange and transportation of nutrients, which is not conducive to long-term cell proliferation. After extensive research, it has been discovered that 3D cell delivery systems (porous microspheres) offer potential solutions to this challenge.

Various techniques, including electrospray, microfluidics, polymerization, and composite emulsification, have been utilized to produce hydrogel microspheres [26]. Among these techniques, microfluidic and electrospray technologies are particularly popular due to their mild gelation conditions, simple and stable production processes, precise control over microsphere size, and ease of MSC entrapment [27,28]. Here, we hypothesized that porous microspheres protect MSCs from immune recognition, maintain cell activity, and enhance immune regulatory function, thus improving the therapeutic effect of liver fibrosis. To prove this hypothesis, we fabricated porous microspheres with different sizes and encapsulated MSCs (Mi-BMSCs) via microfluidic electrospray. We then observed the proliferation, secretion function, and biocompatibility of MSCs inside microspheres, and investigated the efficacy and mechanism of anti-inflammation and anti-fibrosis in two animal models of liver cirrhosis, as shown in Fig. 1. Our data demonstrated that the porous microspheres encapsulated with MSCs could increase MSCs accumulation, prolong retention under systemic administration, and display much more superiority than BMSCs with potential for the treatment of CCl_4 and TAA-induced liver cirrhosis.

2. Experimental procedures

2.1. Materials

Thioacetamide (TAA), carbon tetrachloride (CCl_4) and calcium chloride ($CaCl_2$) were purchased from Aladdin (China). Alginate (ALG) and Polyethylene oxide (PEO) were obtained from Sigma-Aldrich (USA). Rabbit-derived BMSCs, specific medium for rabbit and mouse BMSCs,

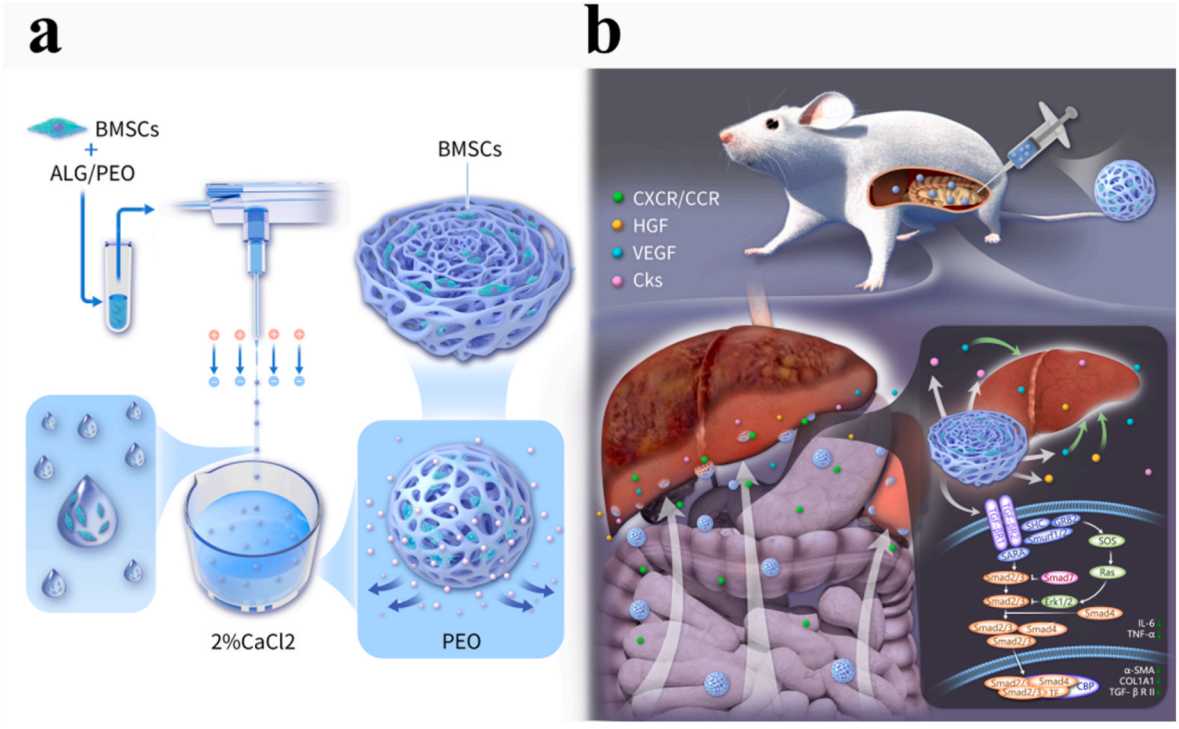

Fig. 1. Schematic illustration of BMSCs-loaded porous particles fabrication. **a.** The generation of porous microcapsules with microfluidic electrospray; **b.** BMSCs-encapsulated microspheres intraperitoneally regulate the inflammatory microenvironment to alleviate liver function and fibrosis through paracrine and TGF-β/Smad signaling pathway for liver cirrhosis.

stem cells adipogenic, osteogenic, and chondrogenic differentiation kits, as well as MSCs surface marker detection kits, were obtained from Oricell (China). Dulbecco's modified Eagle's medium (DMEM), fetal bovine serum (FBS), penicillin-streptomycin (Pen-Strep), and trypsin-EDTA solution were supplied by Gibco (USA). Collagenase D was obtained from Roche (Basel, Switzerland). The cell counting kit-8 (CCK-8) assay kit and D-luciferin were purchased from GLPBIO (USA). LO2 cell, Mouse-derived hepatic stellate cells (HSCs) and a specific medium for mouse HSCs were obtained from iCell (China). Recombinant Human TGF-β1 and Annexin V Apoptosis detection kits were purchased from Peprotech (USA) and MultiSciences Biotech (China), respectively. Luciferase lentivirus was obtained from GeneChem (Shanghai, China). Enzyme-linked immunosorbent assay (ELISA) kits for HGF and VEGF were purchased from Neobioscience (China). ELISA kits for IL-6, IL-1β, IL-10, TNF-α, and TGF-β were obtained from Boyun Biotech (Shanghai, China). The alanine aminotransferase (ALT) Assay Kit, Aspartate aminotransferase (AST) Assay Kit, Total bilirubin (TBIL) Kit, and Hydroxyproline Kit were purchased from Jiancheng (Nanjing, China). CD68, IL-1β, TNF-α antibodies were obtained from abcam (UK). PCNA, IL-6, N-Cadherin, E-Cadherin, and TGF-β Fibrosis Pathway Antibody Sampler Kit antibodies were obtained from CST (USA). Vazyme Biotech Co. (China) provided total RNA kits, two-step QRT-PCR kits, and 2 × Taq Pro Universal SYBR Green Master Mixes.

2.2. Isolation and characterization of BMSCs

A typical procedure was followed to isolate BMSCs from 4-week-old BALB/c male mice [29]. First, the tibias and femurs were sheared using surgical scissors, washed with DMEM three times, and chopped up. Then, they were incubated with collagenase D (1 mg/mL) at 37 °C for 1 h in a shaker. The resulting precipitates were treated with red blood cell (RBC) lysis buffer for 5 min and washed with PBS three times. Finally, the precipitates were plated in culture flasks with BMSCs complete medium. The BMSCs were cultured in a specific medium at 37 °C in a humidified incubator with 5 % CO_2. When the confluence reached 80 %, the cells were passaged. Cells within passages 3 to 6 (P3–P6) were used for further experiments.

The isolated BMSCs were identified by flow cytometric analysis and *in-vitro* differentiation assay. For flow cytometric analysis, a total of 1 × 10^5 BMSCs were collected in each tube and incubated with different primary cell surface marker antibodies (CD29, CD31, CD34, CD44, CD105, CD117, Sca-1) for 30 min in the dark. Flow cytometric analysis was performed after washing the stained cells with PBS. For the differentiation assay, BMSCs were plated into 6-well plates at a density of 2 × 10^5/well. The differentiation media for adipogenesis, osteogenesis, or chondrogenesis were added after 80 % confluence. A three-week induction period was followed by a PBS wash and 20 min fixation in 4 % paraformaldehyde. For staining, Oil Red O solution was applied for 10 min at room temperature, Alizarin Red S solution for 30 min at 37 °C, and Alcian Blue solution for 1 h. Stained cells were observed under a microscope.

2.3. Preparation and characterization of the porous microspheres and Mi-BMSCs

The porous microspheres were prepared using the ALG/PEO precursor solution via microfluidic electrospray. In brief, ALG powder (0.1 g) and PEO (0.01g) were added into deionized water (ddH_2O) (10 mL) and stirred by vortex mixer (1000 rpm) for 4 h at 37 °C to ensure ample dissolution. Then, ALG/PEO solution was injected through a capillary with a tapered tip of 200 μm and delivered to microfluidic electrospray to generate droplets continuously with the voltage of 7 kV and the flow rate of 150 μl/min at room temperature. Next, the droplets were dropped into a $CaCl_2$ (2 wt%) solution for solidification and the PEO solution was removed to create the porous structure of the microspheres. Finally, the ALG microspheres were obtained and washed with ddH_2O water three times for the next experiment.

The BMSCs were mixed with ALG/PEO solution at a density of 5 × 10^6/ml. The mixture (BMSCs and ALG/PEO solution) was then passed through an electric injection device to generate droplets through the electrostatic force, which were subsequently dropped into a $CaCl_2$ (2 wt %) solution at room temperature. Rapid solidification occurred, resulting in the formation of microspheres loaded BMSCs (Mi-BMSCs) in the$CaCl_2$ (2 wt%) solution. Importantly, Mi-BMSCs were obtained and washed three times with DMEM immediately. Diluting 100 μL of ALG microspheres and Mi-BMSCs solution into 1 mL of PBS, the particle size and surface zeta potential were examined using a Zeta-sizer Nano ZS instrument (Malvern, UK). The morphology of the microspheres was examined and captured using an optical microscope, and the size of the microspheres was measured using Image J software. The 3D porous microcapsules were freeze-dried and coated with gold before being analyzed with a scanning electron microscope (FE-SEM, Hitachi, SU8010) to characterize their microstructures. The Mi-BMSCs were fixed with 2.5 % glutaraldehyde, quickly frozen with liquid nitrogen, and connected with refrigerated transmission system (Quorum PP3010) and Energy spectrum (Oxford AZtecLive UltimMax 100) before being analyzed with High resolution field emission scanning electron microscope system (Cryo-SEM, Hitachi, Regulus 8220). The specific surface area and pore size distributions of the porous microspheres were determined using a fully automated Brunauer–Emmett–Teller (BET) surface (volume) analyzer (Micromeritics ASAP 2460, USA).

2.4. The degradation and biocompatibility of porous microparticles in vivo

For degradation research *in vivo*, a piece of ALG hydrogel (100 mg) was implanted into abdominal cavity in mice. The hydrogel piece was collected from abdominal cavity to measure their weight at day 3, 7, 10 and 14. The serum and heart, liver, spleen, lung, and kidney tissues were collected for subsequent experiments at day14.

2.5. Biocompatibility of porous microparticles in vitro

To evaluate the biocompatibility of the porous microparticles on BMSCs, LO2 and HSCs, CCK-8 and live staining assays were conducted. For the CCK-8 assay, a density of 5 × 10^3 BMSCs, LO2 and HSCs per well were seeded in 96-well plates. After cell adhesion, the cells were incubated with different concentration of cell-free porous microparticles and complete medium for 24 h and 48 h. Following the removal of the microparticles and medium, 10 μL of CCK-8 solution was added to each well and incubated for an additional 2 h at 37 °C. The optical density at 450 nm was measured using a microplate reader. For the live-staining assay on BMSCs, LO2 and HSCs, a 6-well plate was utilized. BMSCs, LO2 and HSCs were cultured with 8 % cell-free porous microparticles for 48 h and then stained with 2 μM Calcein-AM at 37 °C for 30 min. Fluorescence images of the stained cells were captured using a fluorescence microscope (Leica, USA).

2.6. Cell proliferation of BMSCs and Mi-BMSCs

To compare the proliferation of BMSCs and Mi-BMSCs, a density of 5 × 10^3 BMSCs and Mi-BMSCs per well was seeded in 96-well plates. At different time points, 10 μL of CCK-8 solution was added to each well and incubated for an additional 2 h at 37 °C, and measured at 450 nm. For the live-staining assay on Mi-BMSCs, a 6-well plate was utilized. Mi-BMSCs were cultured for specific time points (1, 3, 7, and 14 days) and then stained with 2 μM Calcein-AM at 37 °C for 30 min. Fluorescence images of the stained cells were captured using a fluorescence microscope.

2.7. ELISA

Adding 100 μl Mi-BMSCs to 1 ml sodium citrate solution (55 mmol/L), which was blended for 1 min to completely dissolved Mi-BMSCs, then centrifuging and counting the BMSCs. A total of 1×10^6 BMSCs and Mi-BMSCs were cultured for 1, 3, and 5 d. Subsequently, the culture supernatants of both BMSCs and BMSC-laden microspheres were collected. Following the instructions provided with the ELISA kits, the levels of HGF and VEGF in the supernatants without being diluted were measured. The absorbance at 450 nm was determined using a microplate reader.

2.8. In-vitro activation of hepatic stellate cells

HSCs were cultured in a specific medium with 10 % FBS and 1 % Pen-Strep solution. A total of 2×10^5 HSCs were seeded in 6-well plates. The cells were grown overnight in a serum-deprived medium. Afterward, the activated phenotype of HSCs was formed by incubation with TGF-β1 (10 ng/mL) for 24 h. Co-culturing of activated HSCs with Mi-BMSCs or BMSCs was performed for 24 h. For the apoptosis assays, cells were collected and stained with 5 μL Annexin V-FITC and 10 μL propidium iodide (PI) solution. Cells were incubated for 5 min at room temperature and analyzed by flow cytometric analysis (Beckman, USA).

2.9. In vivo biodistribution and residence of Mi-BMSCs

To assess the distribution and persistence time of Mi-BMSCs *in vivo*, BMSCs were first transfected with luciferase lentivirus (MOI = 100). Male Balb/c mice were randomly divided into four groups, and BMSCs or Mi-BMSCs were injected intraperitoneally or intrasplenically, respectively. The number of BMSCs injected in each group was 1×10^6 in 200 μL PBS. After intraperitoneal injection of 3 mg D-luciferin, the mice were imaged using a bioluminescence system (IVIS Lumina) at various time points (1, 3, 7, and 14 days).

2.10. In vivo therapeutic effect of Mi-BMSCs for liver cirrhosis

Six-week-old male Balb/c mice were purchased from Zhejiang Vital River Company (China). The mice were housed at the First Affiliated Hospital of Wenzhou Medical University under specific pathogen-free (SPF) conditions. All rabbits were individually housed in steel cages at the Wenzhou Institute, University of Chinese Academy of Sciences Laboratory Animal Center under standard feeding conditions throughout the experimental period. All animal experiments were conducted in accordance with the rules of the Animal Ethical and Welfare Committee of the First Affiliated Hospital of Wenzhou Medical University (WYYY-AEC-2021-316) and the Ethics Committee of Wenzhou Institute, University of Chinese Academy of Sciences (IUCAS22091901). Liver cirrhosis models were established according to a standard protocol [30,31]. In mice, the dose of TAA was 100 mg/kg in the first week, followed by 200 mg/kg twice a week in the second week and subsequent weeks, 300 mg/kg in the third to fourth weeks, and 400 mg/kg for a total of six weeks. For rabbits, CCl_4 diluted in mineral oil (1:1) was injected intraperitoneally once every three days for 8 weeks (0.2 mL/kg). The animals with liver cirrhosis were randomly divided into three groups (6 mice and 4 rabbit each group), which were treated with PBS. BMSCs and Mi-BMSCs (1×10^6 cells/mice, 5×10^6 cells/rabbit) were injected intraperitoneally in 400 μL PBS after modeling. After treatment, all mice and rabbits were sacrificed at the seventh and ninth weeks, respectively. Liquid nitrogen was used to freeze the serum and the heart, liver, spleen, lung, and kidney tissues for subsequent experiments.

The heart, liver, spleen, lung, and kidney tissues were subjected to deparaffinization, hydration, and sectioning at a thickness of 5 μm. To evaluate the extent of liver fibrosis, histological staining techniques including H&E, Masson's trichrome, as well as immunohistochemical (IHC) and immunofluorescent (IF) staining of liver tissues were performed. For immunohistochemistry, α-SMA antibody (1:200) and PCNA antibody (1:2000), E-Cadherin antibody (1:400), N-Cadherin antibody (1:200), CD68 antibody (1:200) and IL-6 antibody (1:100) were used. For immunofluorescent staining, α-SMA antibody (1:200) and TGF-β antibody (1:100) were used.

2.11. Western blotting

Total proteins were isolated from liver tissues and HSCs. Western blot analysis was performed to investigate the levels of IL-1β, TNF-α, IL-6, α-SMA, COL1A1, Epithelial–mesenchymal transition (EMT) related proteins (N-cadherin, E-cadherin), and TGF-β/Smad signaling pathway proteins. The protein levels were normalized to β-actin and GAPDH as reference proteins.

2.12. qRT-PCR

Total RNAs from livers were isolated using an RNA simple Total RNA Kit. qRT-PCR was performed with a commercial two-step kit and analyzed using 2 × Taq Pro Universal SYBR Green Master Mix. The mRNA levels of α-SMA, COL1A1, TGF-β, IL-6, TNF-α, IL-1β and IL-10 were examined by qRT-PCR using a 7500 Fast Real-Time PCR System (Applied Biosystems). GAPDH was used as an endogenous control for normalization. Table 1 lists the primer sequences used in this study.

2.13. Cytokine assay and serum measurements

To evaluate the inflammation level in livers after Mi-BMSC treatment, ELISA was performed to detect the levels of TNF-α, TGF-β, IL-6, IL-1β and IL-10 with serum samples being diluted following the manufacturer's instructions. Additionally, serum levels of total bilirubin (TBIL), aspartate aminotransferase (AST), and alanine aminotransferase (ALT) were measured to assess hepatic damage and function, according to the manufacturer's protocols. Furthermore, the degree of liver fibrosis was evaluated by measuring hydroxyproline levels in the serum.

2.14. Statistical analysis

Data were analyzed using GraphPad Prism 8.0 software (GraphPad, USA), and graphs were constructed using Origin 2018 software (OriginLab, USA). All data are presented as Mean ± SD. Comparisons between groups were performed using Student's t-test or ANOVA analysis. Statistical significance was determined by a p-value of less than 0.05.

3. Results and discussion

3.1. Characterization of ALG microspheres and Mi-BMSCs via microfluidic electrospray

ALG, a water-soluble substance separated from algae, is commonly employed in the preparation of microsphere particles. This is attributed to its gentle sol-gel process, straightforward curing method, excellent biocompatibility, and non-toxic nature. PEO, in contrast, serves as a pore-forming agent. It is a water-soluble polymer that is non-toxic and exhibits remarkable flocculation effects. Moreover, PEO is insoluble in CaCl2, thereby reducing friction resistance in fluid turbulence. In a typical experiment, a mixture of BMSCs and ALG/PEO solutions was pumped into a microfluidic electrospray assay via a syringe pump. The microfluidic electrospray chip used in this process consisted of a syringe needle with a flat-cut glass capillary (Figure S1), enabling the generation of porous microparticles. At the outlet of the high-voltage direct current (HVDC) device, a "Taylor cone" was formed, and the precursor mixture comprising ALG and PEO underwent droplet formation as it descended (Figure S1). These droplets were collected and subsequently solidified in 2 % $CaCl_2$ solution. The resulting microspheres were then observed under a microscope (Figure S2). The size of the microspheres can be

Table 1
Primers used in qRT-PCR to evaluate gene expression.

Gene	Forward primer sequence	Reverse primer sequence
mos-ACTA1	CCCAAAGCTAACCGGGAGAAG	GACAGCACCGCCTGGATAG
mos-COL1A1	GCTCCTCTTAGGGGCCACT	ATTGGGGACCCTTAGGCCAT
mos-TGF-β	CCAGATCCTGTCCAAACTAAGG	CTCTTTAGCATAGTAGTCCGCT
mos-IL-6	CTTCTTGGGACTGATGCTGGTGAC	TCTGTTGGGAGTGGTATCCTCTGTG
mos-TNF-α	GGACTAGCCAGGAGGGAGAACAG	GCCAGTGAGTGAAAGGGACAGAAC
mos-IL-10	TGCCAAGCCTTATCGGAAATGATCC	AGCCGCATCCTGAGGGTCTTC
mos-IL-1β	CACTACAGGCTCCGAGATGAACAAC	TGTCGTTGCTTGGTTCTCCTTGTAC
mos-GAPDH	GGCAAATTCAACGGCACAGTCAAG	TCGCTCCTGGAAGATGGTGATGG

adjusted by manipulating various parameters, such as the flow rate of the syringe pump, voltage, and the diameter of the glass capillary. With increasing in voltage, the microsphere sizes were progressively decreased, whereas an increase in the flow rate resulted in larger microspheres (Figure S3).

The superficial porous structure of the formed microparticles was examined using a scanning electron microscope (Fig. 2a and b). To prove that BMSCs are successfully loaded by microspheres and observe the internal structure of Mi-BMSCs, the mixture of BMSCs, ALG, and PEO was prepared and injected into the electrospray chip using a microfluidic pump, resulting in the formation of Mi-BMSCs in situ under the HVDC device (Fig. 1a), then stored and cultured in the special DMEM for

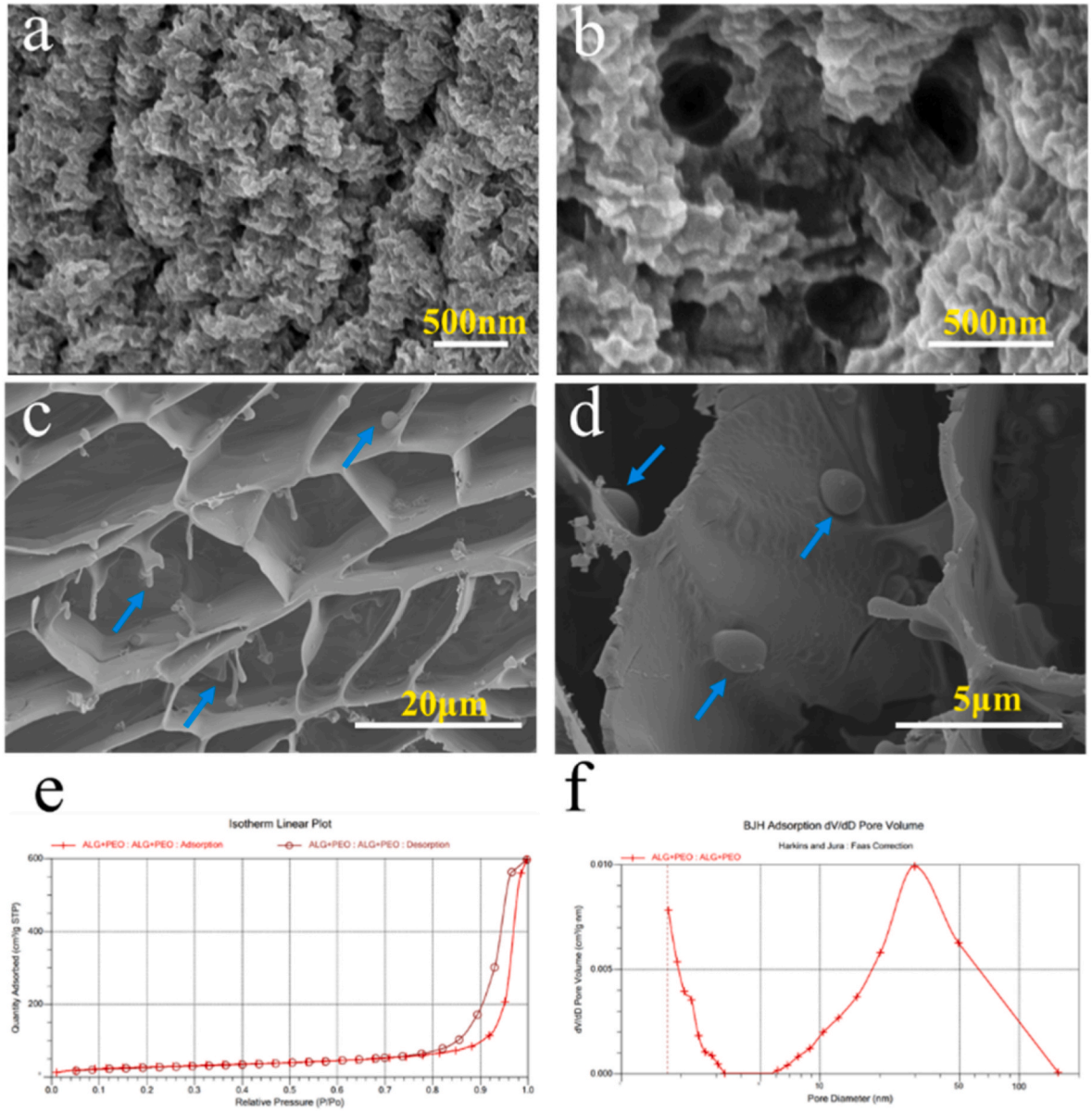

Fig. 2. Characterization of ALG microspheres via microfluidic electrospray. **(a, b)** The structure of the porous microparticles under a scanning electron microscope (SEM). **(c, d)** The representative images of the microparticles loading BMSCs under different magnification by a biocryo-scanning electron microscope (Cryo-SEM). The blue arrows point at the BMSCs. **(e, f)** Adsorption–desorption isotherm and pore-size distribution of porous microspheres.

subsequent experiments. As shown in Fig. 2c–d and Figure S4, ALG microspheres had numerous interweaved pore structure, which provided adequate space to loaded BMSC cells, and were benefit to nutrient exchange for the survival of BMSCs. In addition, the size of Mi-BMSCs were little larger than microspheres (Figure S5a-c). The Zeta potential of microsphere was negatively charged, and that of Mi-BMSCs was more negative (Figure S5d). The BET analysis revealed a specific surface area of 102.5925 ± 0.1642 m^2/g, indicating a considerable surface area available for interactions. The microspheres exhibited pore sizes of approximately 50 nm, and the pores appeared to be spherical in shape (Fig. 2e and f). These findings collectively demonstrate that the porous structure facilitates the acquisition of oxygen and nutrients by BMSCs, as well as the removal of metabolic waste, thereby promoting cell proliferation and secretion. Additionally, these results provide evidence for the successful loading of BMSCs within the microspheres.

3.2. The identification and characters of primary mouse BMSCs

Numerous studies have indicated that bone marrow-derived mesenchymal stem cells (BMSCs) hold significant potential for the treatment of liver cirrhosis [32,33]. In this study, BMSCs were isolated from mouse bone marrow following established protocols commonly

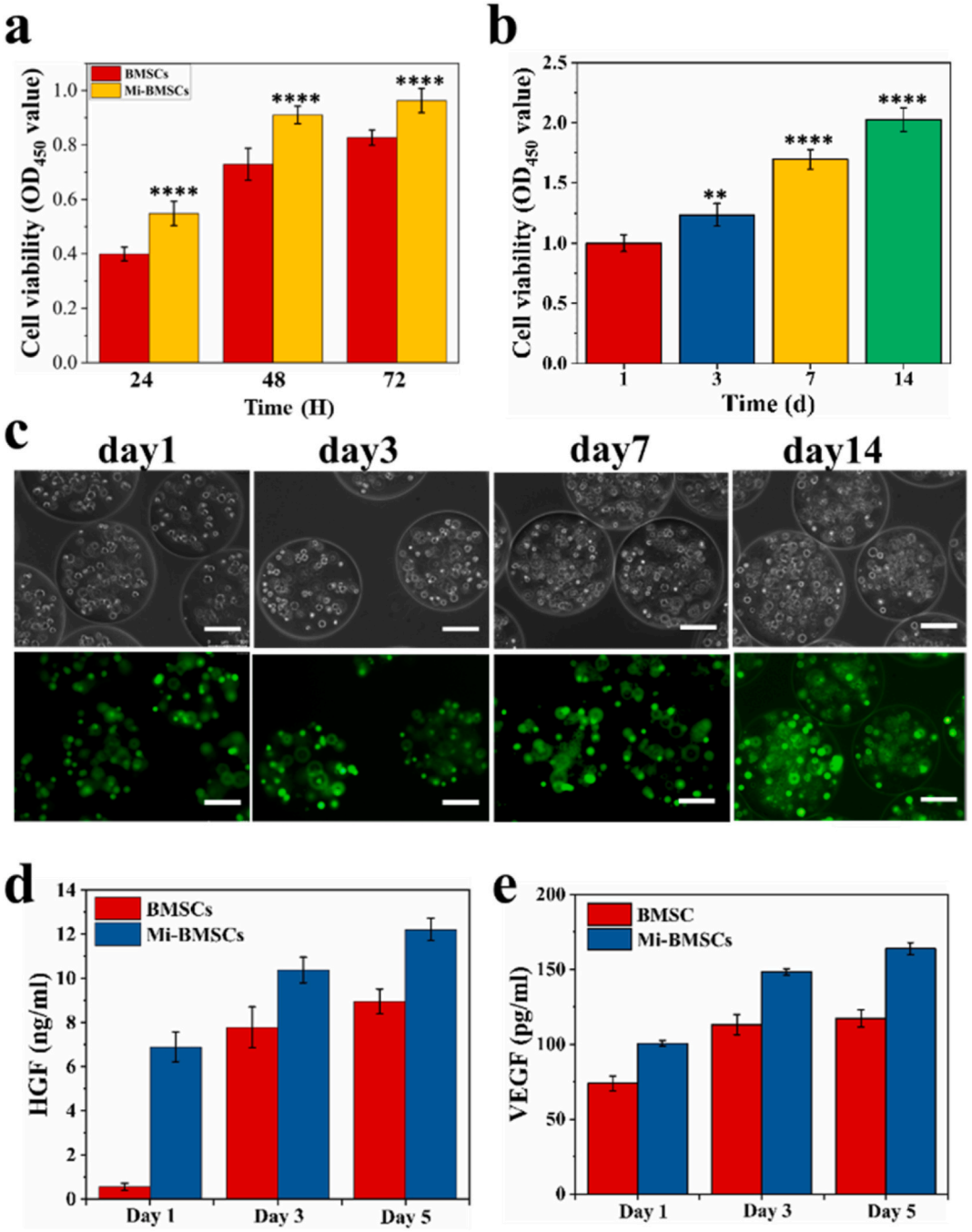

Fig. 3. Proliferation and secretion function of Mi-BMSCs. **(a)** The cell viability of BMSCs and Mi-BMSCs at 24h, 48h, 72h. ****p < 0.0001 vs BMSCs group. **(b)** The viability of Mi-BMSCs at day 1, 3, 7, and 14. **p < 0.01, ****p < 0.0001 vs day1 group. **(c)** Representative images of Mi-BMSCs at day 1, 3, 7, and 14 recorded by optical or fluorescence microscopy. Scale bar = 100 μm. **(d, e)** The HGF **(d)** and VEGF **(e)** levels in BMSCs or Mi-BMSCs supernatant detected by ELISA. Data are expressed as Means ± SD. ****p < 0.0001 vs BMSCs group.

employed for this purpose. To verify that the primary mouse BMSCs accord with the experimental requirements, as shown in Figure S6, adherent BMSCs displayed a spindle-shaped fibroblast morphology at P0, P1, P3, and P7. To confirm the pluripotency of BMSCs, the differentiation abilities of BMSCs for adipogenesis, osteogenesis, and chondrogenesis *in vitro* were assessed. Figure S7 demonstrated that BMSCs can differentiate into osteoblasts, adipocytes, and chondrocytes under specific differentiation-inducing conditions *in vitro*, exhibiting distinct calcium granules, oil droplets, and cartilage particles, respectively. In addition, flow cytometry analysis, as depicted in Figure S8, proved that positive expression of stemness markers CD29, CD44, CD105, and Sca-1 were >95 % in the isolated mouse BMSCs. Conversely, the expression levels of hematopoietic markers CD31, CD34, and CD117 were found to be low (<2 %). These findings align with the characterization criteria established by the International Society for Cell Therapy (ISCT) for mouse MSCs [34]. Based on these results, it can be inferred that the primary mouse BMSCs obtained in this study are suitable for subsequent experimental investigations.

3.3. The biocompatibility of ALG microparticles in vitro and in vivo

Then, the biocompatibility of the microparticles with BMSCs was evaluated using CCK-8 and *in vitro* living-staining assays. As depicted in Figure S9a-9f, no significant differences in LO2, HSCs and BMSCs viability were observed after co-culturing with different concentration of microparticles for 24 and 48 h by CCK-8 and living-staining assays. To prove the safety of porous microparticles *in vivo*, there were no perceptible damages in the major organs of mice collected from two groups by the H&E staining and liver function (AST, ALT and TBIL), as shown in Figure S10. These results suggested the superior biocompatibility of ALG microparticles *in vitro* and *in vivo*.

3.4. The proliferation and function of BMSCs-loaded in ALG microspheres in vitro

To further evaluate the benefits of ALG microspheres as a cell delivery system, we compared the cell viability of BMSCs and Mi-BMSCs at 24 h, 48 h, 72 h. As shown in Fig. 3a, the CCK-8 results showed that Mi-BMSCs proliferated more significantly than BMSCs at 24 h, 48 h and 72 h. In addition, Fig. 3b demonstrated a gradual increase in the viability of Mi-BMSCs over time ($p < 0.001$), and as depicted in Fig. 3c, the *in vivo* staining assay demonstrated robust growth of BMSCs within the porous microparticles during a 14 days culture period, indicating that the porous ALG microspheres supported the growth and viability of BMSCs during long-term culture. Furthermore, we assessed the cytokine secretion function of pure BMSCs and Mi-BMSCs using ELISA. The findings revealed that both pure BMSCs and Mi-BMSCs consistently secreted HGF and VEGF. Notably, the levels of secreted HGF and VEGF were significantly higher in Mi-BMSCs compared to BMSCs (Fig. 3d and e).

Collectively, these results indicate that porous microspheres provide a supportive environment for the growth and proliferation of BMSCs while enhancing their secretory and regulatory functions. In recent years, various 3D cell cultures models, such as organ-on-a-chip, organoids, and spheroids, have been developed, offering valuable tools for studying complex biological systems [35,36]. Nevertheless, these advanced techniques often come with high costs and complex designs, making them less accessible to many researchers. In this study, we have developed a novel approach using porous microspheres that offer a 3D culture environment for MSCs. These microspheres effectively minimize the impact of gravity and provide an optimal setting for cell proliferation and function.

3.5. Mi-BMSCs induced apoptosis of activated HSCs and inhibited the progression of EMT

Activation of hematopoietic stem cells (HSCs) plays a crucial role in the progression of liver cirrhosis. Interestingly, in liver fibrosis, activated HSCs undergo spontaneous apoptosis, albeit at a limited rate [3]. Therefore, enhancing the apoptosis of activated HSCs could be beneficial in alleviating liver cirrhosis. In our study, we observed that neither BMSCs nor Mi-BMSCs had no impact on the proliferation of HSCs *in vitro* (Fig. 4a). However, both BMSCs and Mi-BMSCs promoted apoptosis of activated HSCs (Fig. 4b and c). Furthermore, the relative expression levels of α-SMA, TGF-β, and IL-6 in activated HSCs were significantly reduced following treatment with Mi-BMSCs and BMSCs (Fig. 4d–f). Indeed, epithelial-mesenchymal transition (EMT) is induced by the activation of HSCs via TGF-β1 cytokines. In our study, we observed that BMSCs played a significant role in promoting the protein expression of E-cadherin, which is known to alleviate EMT. Furthermore, Mi-BMSCs effectively downregulated key markers associated with liver fibrosis, such as COL1A1, N-cadherin, TGF-β R II, and TGF-β, upregulated the protein expression of E-Cadherin (Fig. 4g–l). These findings suggest that Mi-BMSCs can attenuate liver cirrhosis by inducing apoptosis of activated HSCs, promoting the degradation of extracellular matrix (ECM), and inhibiting the progression of EMT [37,38].

3.6. The degradation in vivo of ALG microspheres and hemolysis assay of BMSCs in vitro

Prior to the *in vivo* study, we evaluated the biological safety of BMSCs using an *in vitro* hemolysis assay (Figure S11). BMSCs with different cell densities did not exhibit any hemolytic effects on RBCs *in vitro*, confirming the hematological compatibility of BMSCs. Therefore, the BMSCs used in this study could be utilized for the treatment of liver cirrhosis. ALG gels microparticles are ionically cross-linked and degrade under physiological conditions [39]. To identify the degradation of ALG gels *in vitro*, as shown in Figure S12, the massive sodium alginate hydrogel was placed in the abdominal cavity and the result showed the massive sodium alginate hydrogel remained approximate 60 % of weight at day 14, which supported the long-time proliferation and function of BMSCs.

3.7. The biodistribution and persistence of BMSCs in vivo

Generally, MSCs are administered via peripheral intravenous injection. However, this route often results in the retention of MSCs in the lungs, where they are quickly eliminated by the immune system [15]. Thus, enhancing the survival time and homing capability of MSCs to disease lesions *in vivo* is crucial for improving the therapeutic efficacy of BMSCs [11]. In this study, we successfully developed fluorescein-labeled BMSCs (Luc-BMSCs). Mi-Luc-BMSCs and Luc-BMSCs were intraperitoneally or intrasplenically injected into mice. The biodistribution and persistence of BMSCs were observed *in vivo* at 2 h, 1 d, 3 d, 7 d, and 14 d using the IVIS system.

As depicted in Fig. 5a, the intraperitoneal administration of Mi-Luc-BMSCs exhibited a longer survival time compared to the free Luc-BMSCs group. The fluorescence intensity of the Mi-Luc-BMSCs group remained detectable until the 14th day, whereas in the free Luc-BMSCs group, it diminished by the 7th day. Fig. 5b showed that there was no significant difference in fluorescence intensity between the two groups when administered intrasplenically, although it was slightly stronger in the Mi-Luc-BMSCs group. However, BMSCs showed limited survival by the 7th day and were completely cleared by the 14th day. More importantly, when comparing the treatment methods, the fluorescence intensity of Luc-BMSCs injected intraperitoneally was stronger and more persistent than those injected intrasplenically, which possibly result from large number of immune cells in the spleen inhibiting the proliferation of BMSCs and rapidly eliminating BMSCs. Based on these experimental

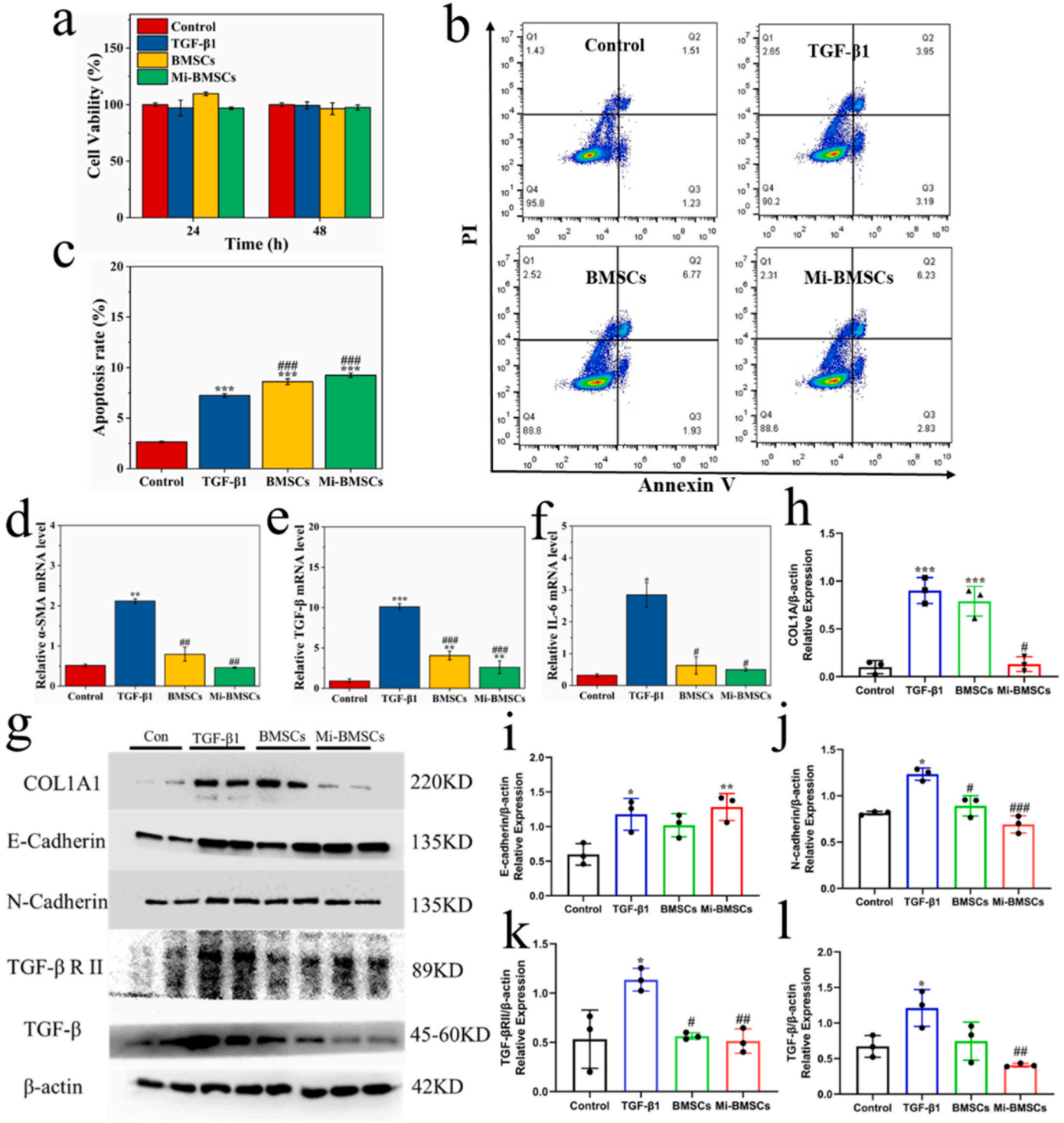

Fig. 4. Therapeutic efficacy of Mi-BMSCs or BMSCs in TGF-β1-induced HSCs activation. (**a**) Cell viability of inactivated HSCs with different treatments at 24h, 48 h. **(b–c)** Total apoptosis of activated HSCs with different treatments at 24 h assayed by flow cytometry analysis (upper and lower right quadrants represent late and early apoptotic cells). **(d–f)** The relative mRNA levels of α-SMA, TGF-β, and IL-6 measured by qRT-PCR in Control, TGF-β1, BMSCs, Mi-BMSCs group. **(g–l)** Western blot and quantification analysis of COL1A1 (**h**), E-cadherin (**i**), N-cadherin (**j**), TGF-β R II (**k**) and TGF-β (**l**) in Control, TGF-β1, BMSCs, Mi-BMSCs group. Data are expressed as Means ± SD. *p < 0.05, **p < 0.01, ***p < 0.001 vs Control group; #p < 0.05, ##p < 0.01, ###p < 0.001 vs TGF-β1 group.

results, intraperitoneal injection was found to be more effective than intrasplenic injection. Therefore, we chose intraperitoneal injection as the preferred method for treating the liver cirrhosis model in subsequent animal experiments.

3.8. *Mi-BMSCs improved liver function and reversed hepatic fibrosis in CCl_4-induced liver cirrhosis*

In our study, we used CCl_4-induced liver cirrhosis rabbits for *in vivo* experiments. The procedure of the animal experiments is illustrated in Fig. 6a. As shown in Fig. 6b, compared to the control group, the livers in

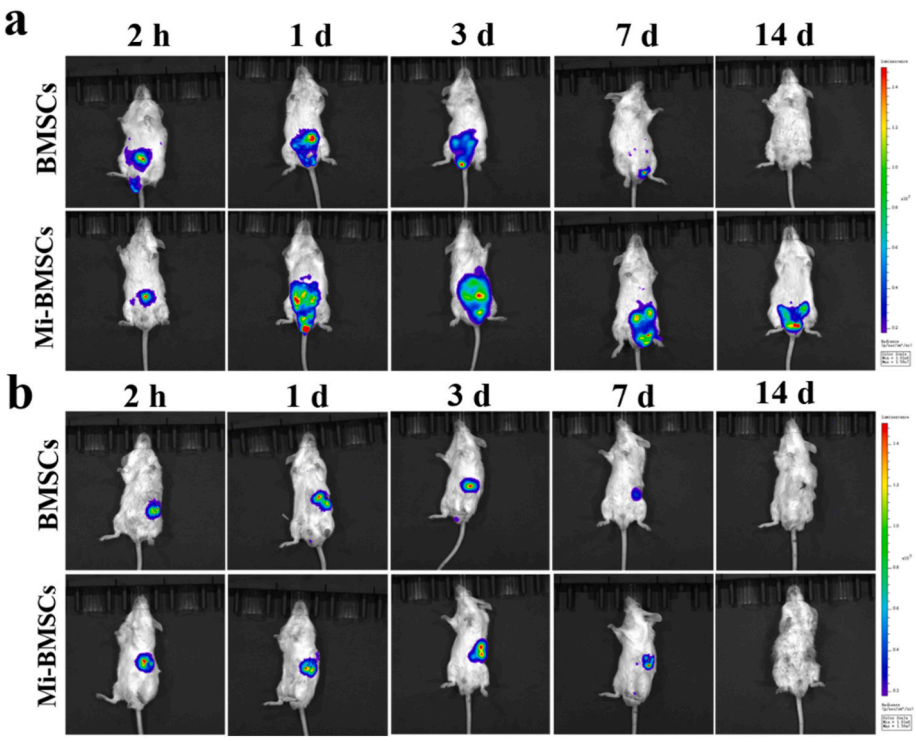

Fig. 5. Biodistribution of BMSCs and Mi-BMSCs *in vivo* at 2 h, 1 d, 3 d, 7 d and 14 d. **(a)** In vivo fluorescence intensity of the mice with Luc-BMSCs or Mi-Luc-BMSCs at different time points after intraperitoneal injection; **(b)** In vivo fluorescence of the mice with Luc-BMSCs or Mi-Luc-BMSCs at different time points after intrasplenical injection.

the CCl_4 group exhibited granular changes and a hardened texture. H&E and Masson staining analysis revealed increased inflammatory cell infiltration, hepatocyte steatosis, necrosis, and pseudo-lobule formation in the CCl_4 group. However, after treatment with Mi-BMSCs, the liver showed a red color, a soft texture, and no inflammatory cell infiltration or fibrous tissue deposition ((Fig. 6b and c). Furthermore, the CCl_4 group showed a significant increase in α-SMA expression, indicating the activation of hepatic stellate cells and the progression of liver fibrosis. In contrast, both the BMSCs and Mi-BMSCs groups exhibited a noticeable decrease in α-SMA expression (Fig. 6b and d). Moreover, compared to the control group, the CCl_4 group demonstrated significant hepatic impairment, as indicated by elevated levels of AST and ALT. However, in the BMSCs and Mi-BMSCs groups, the levels of AST and ALT were markedly decreased (Fig. 6c and d). These findings suggest that Mi-BMSCs have a significant effect on improving liver function and reversing hepatic fibrosis.

3.9. Mi-BMSCs improve liver function and promote liver regeneration in TAA-induced liver cirrhosis

To further evaluate the therapeutic effect of Mi-BMSCs, their potential in ameliorating TAA-induced liver fibrosis was assessed in mice. The experimental procedure is depicted in Fig. 7a. Mi-BMSCs and BMSCs were intraperitoneally injected for 4 and 5 weeks, respectively, into mice with TAA-induced early liver cirrhosis. As depicted in Fig. 7b, the liver in the PBS group exhibited enlargement with granular changes and a hardened texture. In contrast, the livers in the BMSCs and Mi-BMSCs groups displayed a red color, a soft texture, and a relatively smooth surface. Furthermore, H&E staining analysis revealed an increase in inflammatory cell infiltration and bile duct cell hyperplasia in the PBS group (Fig. 7c). Furthermore, the hepatic lobule structure was disrupted, resulting in the rearrangement of hepatic cords and the formation of fibrous septa in the portal areas. Masson staining analyses reveal the presence of pseudo-lobules and a substantial increase in hydroxyproline levels in the liver of the PBS group (Fig. 7d).

Importantly, the disordered structure of hepatic lobules and cords was partially reversed in the Mi-BMSCs and BMSCs groups, indicating the inhibitory effect of BMSCs treatment on fibrosis. Furthermore, treatment with both BMSCs and Mi-BMSCs significantly reduced inflammatory cell infiltration, inhibited connective tissue proliferation, and decreased hydroxyproline levels (Fig. 7e). It is well known that PCNA are important markers of hepatocyte proliferation during the process of liver fibrosis. PCNA expression was slightly upregulated in the PBS group, indicating an active TAA-induced fibrotic process. Interestingly, the levels of PCNA significantly increased after treatment with both BMSCs and Mi-BMSCs, indicating their potential role in promoting liver regeneration and ECM degradation (Fig. 7c and f). Additionally, liver function damage are indeed signs of liver cirrhosis. In comparison to the control group, the PBS group exhibited hepatomegaly and significant hepatic impairment, as evidenced by elevated levels of the liver index, AST, ALT, and TBIL. However, in contrast, the BMSCs and Mi-BMSC groups showed a noticeable reduction in the liver index (liver weight/body weight × 100 %, Figure S13, Fig. 13), as well as decreased levels of AST, ALT, and TBIL (Fig. 7g–i). These results indicate that liver physiologic function was considerably improved in both the BMSCs and Mi-BMSC groups, especially with particle-encapsulated BMSCs.

3.10. Mi-BMSCs suppress fibrosis and the EMT progress in cirrhosis

Fibrous tissue and EMT formation are important markers of liver fibrosis process [5]. A significant increase in α-SMA and N-Cadherin by IHC staining and quantification analysis was observed in the PBS group, whereas obviously decrease were observed in the BMSCs and Mi-BMSC groups (Fig. 8a–d). Conversely, the expression of E-cadherin, a negative regulator of EMT, was upregulated after treatment with BMSCs or Mi-BMSCs (Fig. 8e–f). Moreover, the mRNA and protein relative expression of COL1A1, N-cadherin, E-cadherin, and α-SMA levels by qRT-PCR and WB analysis were significantly alleviated in the Mi-BMSCs group (Fig. 8g–k, Figure S13). Additionally, the fluorescence intensity of α-SMA, as assessed by immunofluorescence staining, also exhibited a

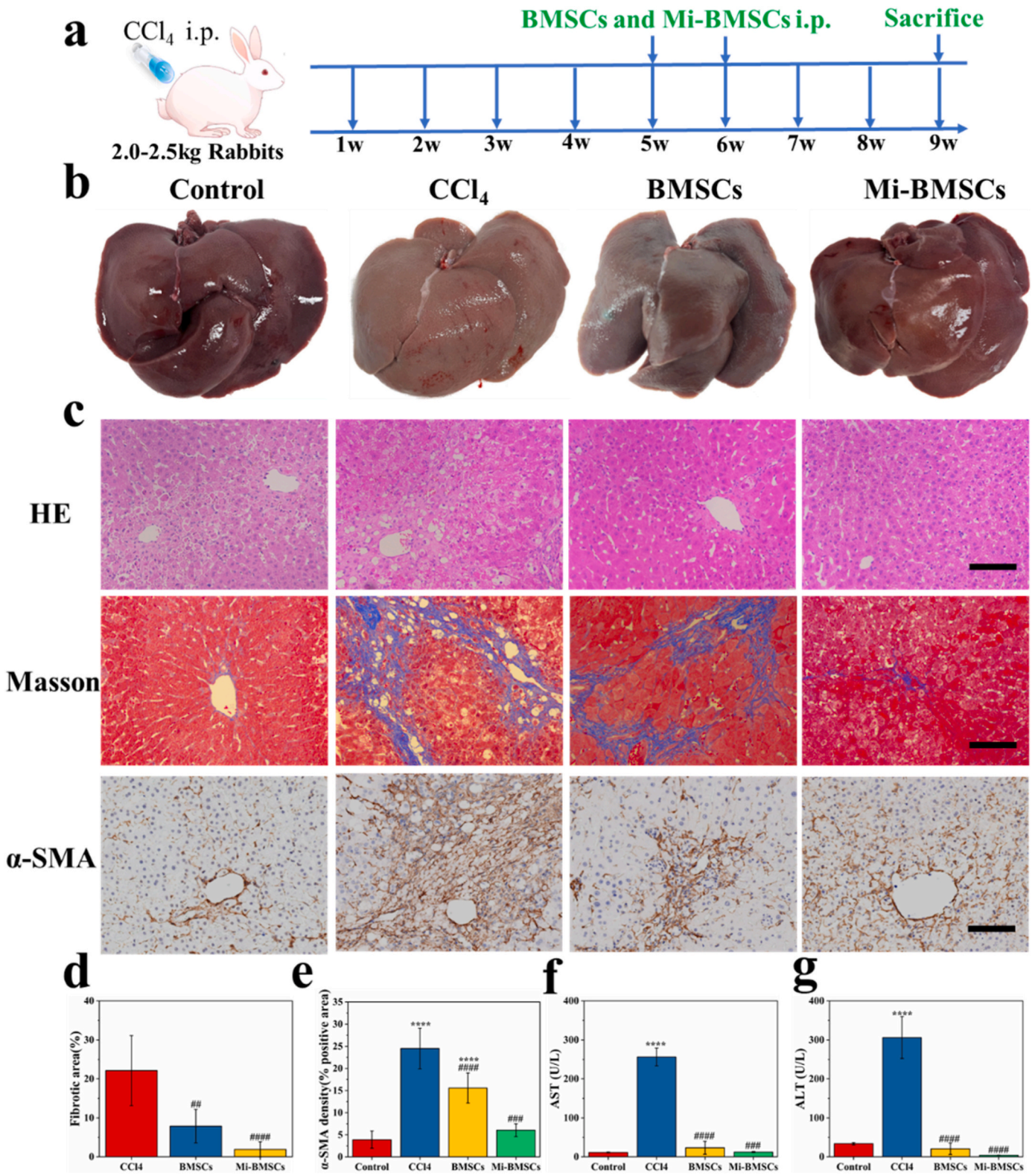

Fig. 6. Therapeutic efficacy of Mi-BMSCs and BMSCs in CCl_4-induced liver cirrhosis rabbits. (**a**) Schematic illustration of animal experiments procedures for 8 weeks actually in CCl_4-induced liver cirrhosis of rabbits. Being treated with PBS, BMSCs and Mi-BMSCs (5×10^6 cells/rabbit) intraperitoneally on days 28 and 35 after modeling. **(b)** Images of liver tissues from the rabbits in Control, CCl_4, BMSCs, Mi-BMSCs group. **(c)** Representative H&E, Masson, α-SMA IHC staining of liver tissues from the rabbits in Control, CCl_4, BMSCs, Mi-BMSCs group. Scale bar = 100 μm. (d) The positive area of fibrosis in liver tissues. **(e)** The quantitative analysis of the α-SMA positive area from liver tissues. Serum AST **(f)** and ALT **(g)** levels in Control, CCl_4, BMSCs, Mi-BMSCs group. Data are expressed as Means ± SD. (*$p < 0.05$, **$p < 0.01$, ***$p < 0.001$, ****$p < 0.0001$ vs Control group, $^{\#\#}p < 0.01$, $^{\#\#\#}p < 0.001$, $^{\#\#\#\#}p < 0.0001$ vs CCl_4 group.

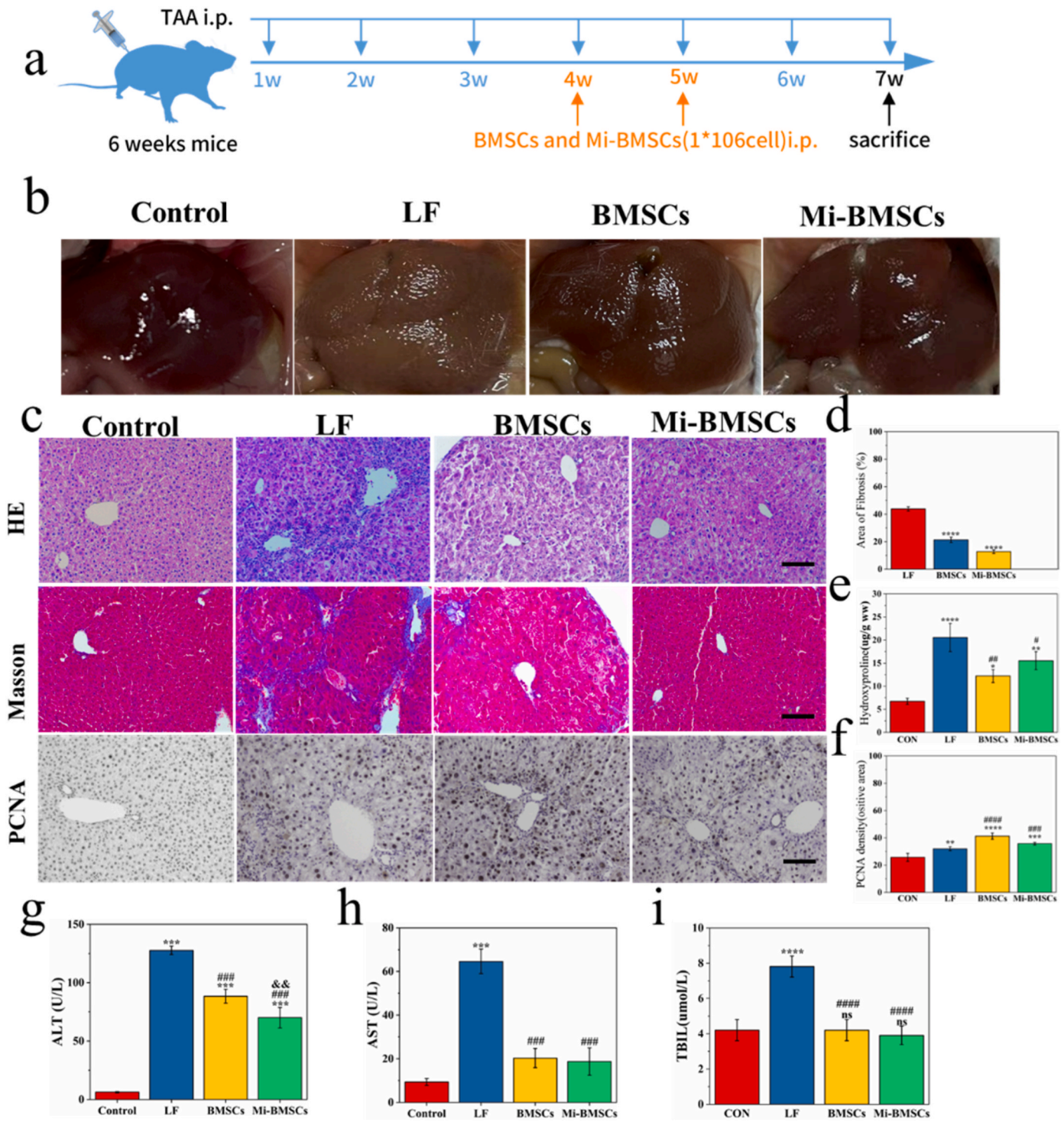

Fig. 7. Therapeutic efficacy of Mi-BMSCs and BMSCs in the TAA-induced liver cirrhosis. **(a)** Schematic illustration of animal experiments procedures for 6 weeks actually in TAA-induced liver cirrhosis. Being treated with PBS, BMSCs and Mi-BMSCs (1×10^6 cells/mice) intraperitoneally on days 21 and 28 after modeling. **(b)** Images of liver tissues from the mice in Control, LF, BMSCs, Mi-BMSCs group. **(c)** Representative H&E, Masson, PCNA IHC staining of liver tissues from the mice in Control, LF, BMSCs, Mi-BMSCs group. Scale bar = 100 μm. **(d)** The fibrosis area of masson staining. (e) Hydroxyproline of liver tissue. **(f)** The quantitative analysis of PCNA positive area in liver tissues. Serum Liver function. **(g)** ALT. **(h)** AST. **(i)** TBIL in Control, LF, BMSCs, Mi-BMSCs group. Data are expressed as Means ± SD. (*p < 0.05, **p < 0.01, ***p < 0.001, ****p < 0.0001 vs Control group, $^{\#\#}$p < 0.01, $^{\#\#\#}$p < 0.001, $^{\#\#\#\#}$p < 0.0001 vs LF group; $^{\&\&}$p < 0.01 vs BMSCs group).

clear reduction in Mi-BMSCs group (Figure S14). Thus, these data declare that Mi-BMSCs suppress fibrosis and the EMT progress in cirrhosis.

3.11. Mi-BMSCs decrease macrophage infiltration and downregulate the expression of inflammatory cytokines

The formation of liver fibrosis involves a complex inflammatory response process that begins with the activation of HSCs, leading to the secretion of inflammatory cytokines and the subsequent development of

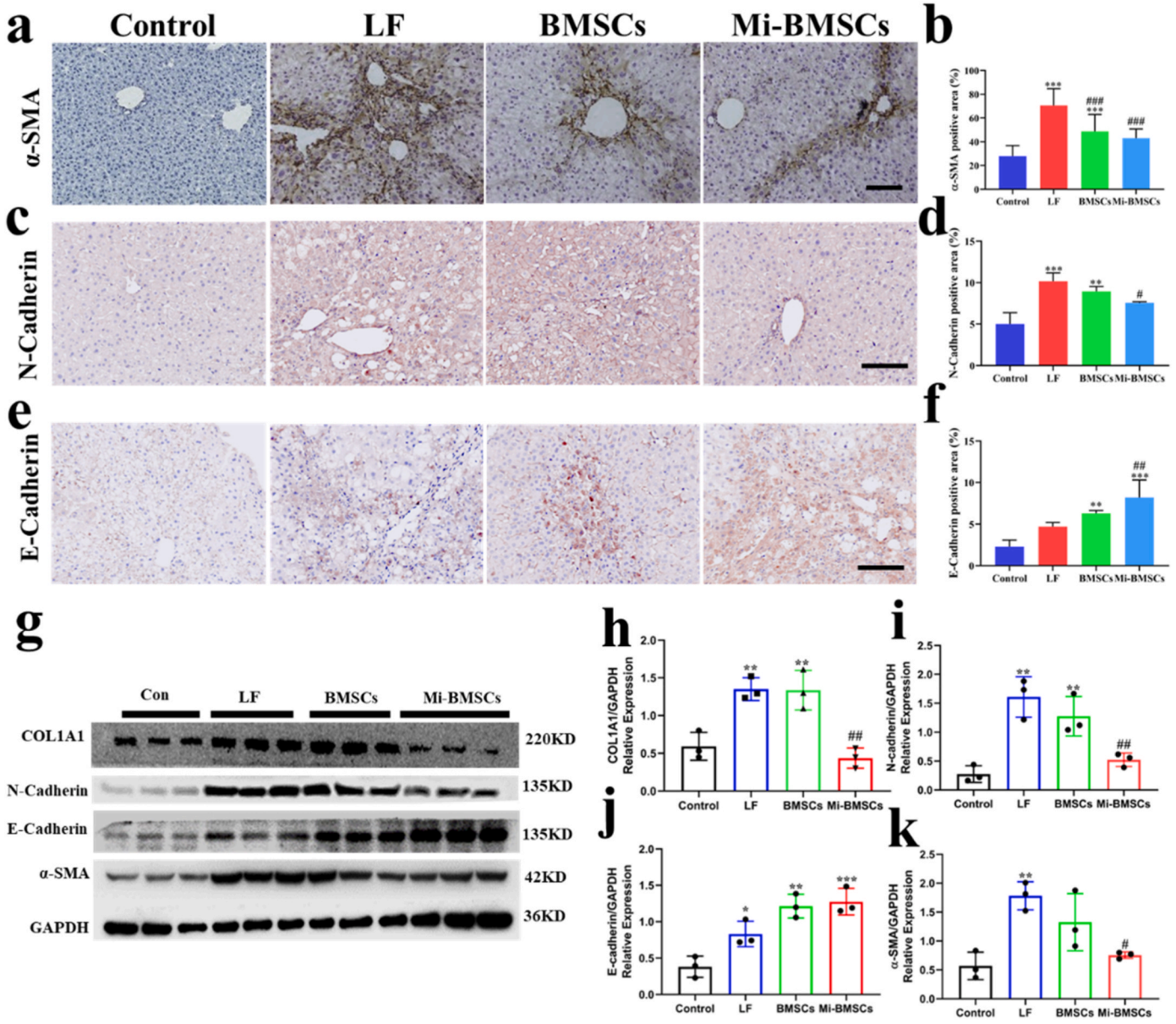

Fig. 8. Suppressing fibrosis and the EMT progress of Mi-BMSCs in the treatment of liver cirrhosis. **(a–b)** Representative α-SMA IHC staining images and quantitative analysis of liver tissues in Control, LF, BMSCs, Mi-BMSCs group. **(c–d)** Representative N-Cadherin IHC staining images and quantitative analysis of liver tissues in each group. **(e–f)** Representative E-Cadherin IHC staining images and quantitative analysis of liver tissues in each group. **(g–k)** The protein relative expression and quantification of COL1A1 **(h)**, N-cadherin **(i)**, E-cadherin **(j)**, and α-SMA **(k)** of liver tissues by WB analysis in Control, LF, BMSCs, Mi-BMSCs group. Scale bar = 100 μm. Data are expressed as Means ± SD. *p < 0.05, **p < 0.01, ***p < 0.001 vs Control group; #p < 0.05, ##p < 0.01, ###p < 0.001 vs LF group.

fibrosis [40]. Infiltration of macrophages plays an important role in inflammatory response. The IHC staining suggested that the expression of CD68 in LF group was significantly increased compared to Control group, whereas that in Mi-BMSCs group was more obvious decreased than BMSCs group (Fig. 9a–b). Subsequently, serum markers of liver function and inflammation levels were measured using ELISA and biochemical detection methods. There was a significant increase in the mRNA expressions of IL-6, TNF-α, IL-1β, IL-10, and protein relative expressions of IL-6, TNF-α, IL-1β in the PBS group, confirming the successful establishment of the liver cirrhosis model (Fig. 9c–n). Following treatment with BMSCs and Mi-BMSC, those mRNA and protein relative expressions showed a significant improvement, particularly in the Mi-BMSC group. Moreover, the serum levels of inflammatory factors (IL-6, TNF-α, IL-1β, and IL-10) were significantly elevated in the PBS group compared to the control group. However, both the Mi-BMSCs and BMSCs groups exhibited a significant amelioration after treatment, with the Mi-BMSCs group showing a particularly pronounced reduction of inflammatory cytokines (Fig. 9g–j). Collectively, the results prove that BMSCs and Mi-BMSCs decrease macrophage infiltration and downregulate the expression of inflammatory cytokines in the treatment of early liver cirrhosis, and the encapsulation of BMSCs within microparticles could enhance this therapeutic effect.

3.12. *Mi-BMSCs attenuate fibrosis in liver cirrhosis through modulation of the TGF-β/Smad signaling pathway*

The TGF-β/Smad signaling pathway plays a crucial role in EMT and the formation of fibrosis. Finally, to investigate the therapeutic mechanism of Mi-BMSCs in the treatment of liver cirrhosis, we examined the proteins expression of TGF-β/Smad signaling pathway through western blotting. Firstly, the fluorescence intensity of TGF-β by IF staining exhibited a clear rise in LF group, but significant reduction in Mi-BMSCs

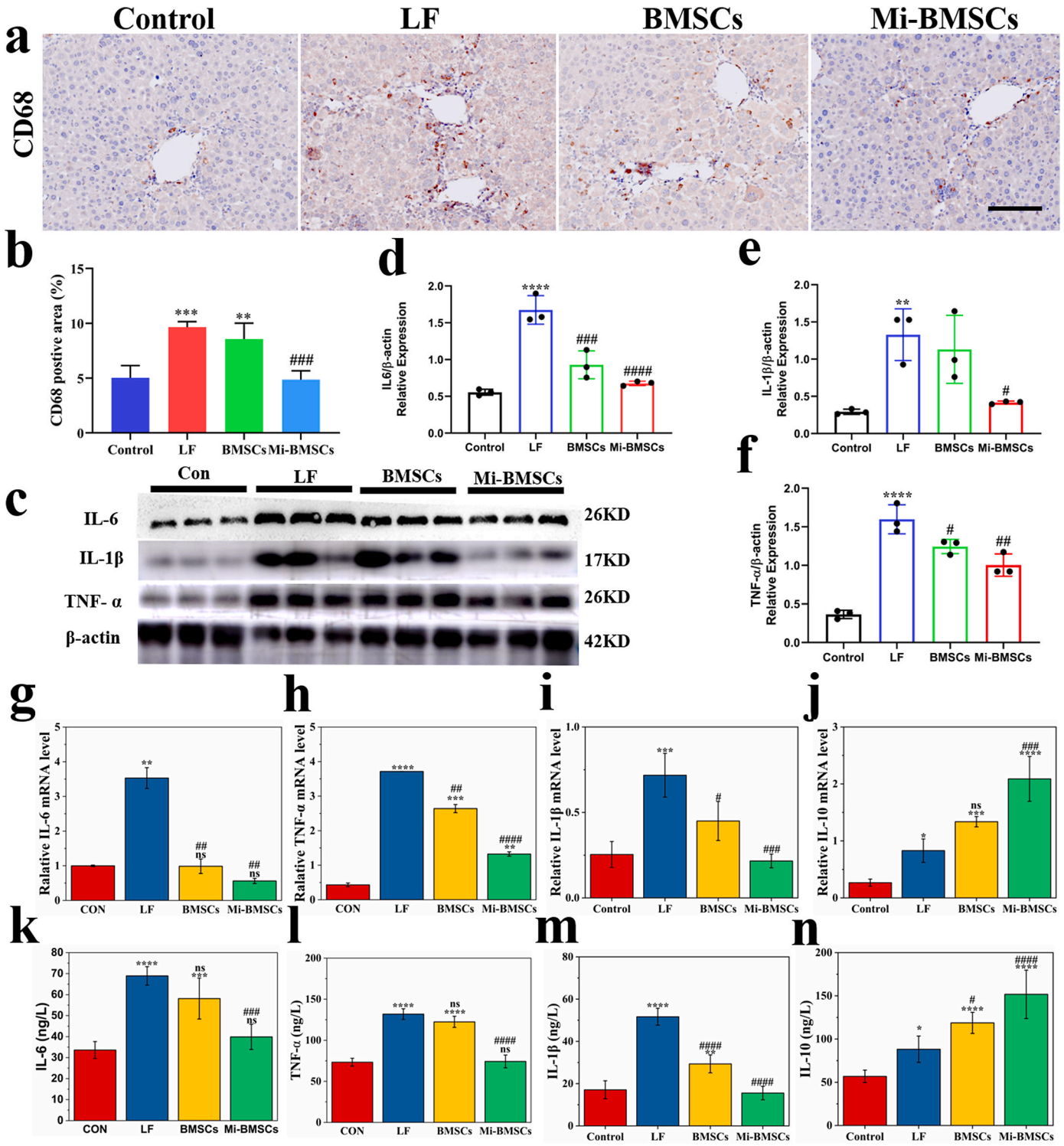

Fig. 9. Mi-BMSCs decrease macrophage infiltration and downregulate the expression of inflammatory cytokines in liver cirrhosis. **(a–b)** Representative IHC staining images and quantitative analysis of CD68 from liver tissues in Control, LF, BMSCs, Mi-BMSCs group. Scale bar = 100 μm. **(c–f)** The protein relative expression and quantification of IL-6 (d), IL-1β (e), TNF-α (f) from liver tissues in Control, LF, BMSCs, Mi-BMSCs group. **(g–j)** The mRNA levels of IL-6 (g), TNF-α (h), IL-1β (i), IL-10 (j) from liver tissues in each group by qRT-PCR assay. **(k–n)** The serum levels of IL-6 (k), TNF-α (l), IL-1β (m), IL-10 (n) in each group by ELISA. *$p < 0.05$, **$p < 0.01$, ***$p < 0.001$, ****$p < 0.0001$ vs Control group; $^{\#}p < 0.05$, $^{\#\#}p < 0.01$, $^{\#\#\#}p < 0.001$, $^{\#\#\#\#}p < 0.0001$ vs LF group; Data are expressed as Means ± SD.

group (Fig. 10a–b), while the results by ELISA and qRT-PCR were consistent (Fig. 10c–d). Subsequently, the results of WB demonstrated that TGF-β/Smad signaling pathway were activated in TAA-exposed liver tissues (LF group), but the expression of TGF-β and the phosphorylation of Smad2/3 and Smad2 were significantly reduced in Mi-BMSC groups (Fig. 10e–h). These findings collectively suggest that Mi-BMSCs alleviate liver dysfunction, suppress inflammation, and attenuate fibrosis in liver cirrhosis through modulation of the TGF-β/Smad signaling pathway.

Recently, MSCs without any carrier are directly injected into a tissue via a syringe or catheter in most clinical trials. Whereas, less than 5 % of injected MSCs persist *in vivo* within days of transplantation, which

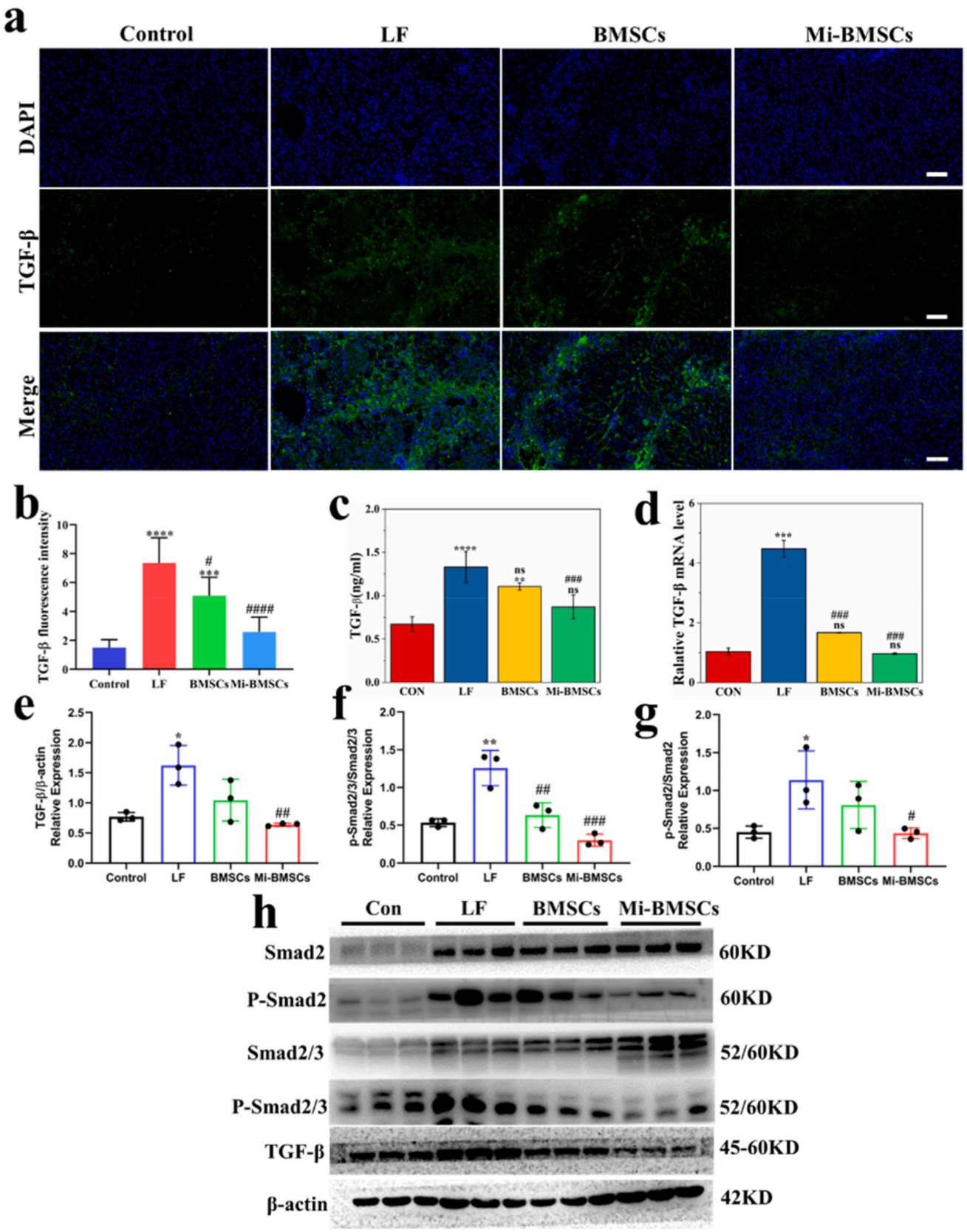

Fig. 10. The mechanism of Mi-BMSCs in the treatment of liver cirrhosis. **(a–b)** The representative fluorescent images and quantification of TGF-β from liver tissues of mice in Control, LF, BMSCs, Mi-BMSCs group by Immunofluorescent (IF) staining. Scale bar = 100 μm. **(c)** The serum levels of TGF-β in each group by ELISA. **(d)** The mRNA levels of TGF-β from liver tissues in each group by qRT-PCR assay. **(e–h)** The protein relative expression and quantification of TGF-β (**g**), the phosphorylation of Smad2 (**f**) and Smad2/3 (**g**) of liver tissues in Control, LF, BMSCs, Mi-BMSCs group by WB analysis *$p < 0.05$, **$p < 0.01$, ***$p < 0.001$ vs Control group; $^{\#}p < 0.05$, $^{\#\#}p < 0.01$, $^{\#\#\#}p < 0.001$ vs LF group; Data are expressed as Means ± SD.

greatly reduces the curative effect of MSCs. Interestingly, MSC encapsulation technologies not only solved this problem, but also enhanced the efficacy and differentiation potential of MSCs. Hamilton et al. [41] designed a separable 3-D co-culture laminates by laminating PEG-based hydrogels with enzyme-degradable hydrogel adhesives, enabling co-culture effects and cultivation to examine the persistence of paracrine signals and provided great potential for the future study of various basic cell signals. Zhao et al. [42] reported a rat-BMSCs encapsulated photo-crosslinkable methacrylated gelatin (GelMA) microspheres process that utilized this technology to facilitate bone regeneration with minimum invasion, showing enhanced osteogenesis *in vitro* and *in vivo*. Gao et al. [43] developed a bioprinted PEG-GelMA composite scaffold layer by layer to introduce a 3D structure for embedding MSCs, confirming the osteogenesis and chondrogenesis of the MSCs for 21 days. Although these new technologies provide various possibilities for the treatment of MSC, the preparation process is complicated and the injection mode is limited, mainly for local treatment to achieve the synergistic effect of stem cells. Therefore, there is still a lack of research on systemic application and liver cirrhosis.

In our research, the delivery system of porous microspheres loaded with BMSCs was completed by microfluidic technology, which controlled the size of microspheres and facilitate direct injection, and was applied to systemic and local treatment. Using high molecular weight hydrogel for porous microspheres can increase the mechanical properties of the gel and improve the viscosity of the gel to reduce the mechanical damage for BMSCs during preparation. It has superior biocompatibility and stability, can provide enough space for the proliferation of BMSCs through pore structure, promote the exchange of nutrients to benefit for the long-term survival and function of BMSCs. Additionally, porous microspheres are used as a drug carrier to realize the rapid transportation and exchange of cytokines. The encapsulated BMSCs can reduce the recognition of immune cells, prolong the persistence time *in vivo*, thus reducing the number of patients' transfusion and the cost in hospital. However, the manufacturing process is a little complicated, and difficult to prepare in large quantities. Although the content of PEO involved is low, it will be swallowed up by cells at the same time when preparing the cell delivery system, which has certain immunogenicity. Secondly, BMSCs are time-consuming, expensive and difficult to obtain clinically. Heterologous transplantation has ethical problems and some unknown side effects, so more related experiments are needed to further verify and provide theoretical basis in the future.

4. Conclusion

In this study, we developed a novel approach for the treatment of early liver cirrhosis by preparing porous microspheres with BMSCs using microfluidic electrospray. These porous microspheres offered an improved 3D culture environment and demonstrated compatibility with BMSCs. The unique pore structure of the microspheres facilitated efficient nutrient exchange and cytokine secretion, thereby preserving the biological activity of the cells, and preventing their clearance by immune cells. Importantly, the encapsulation of BMSCs within the porous microparticles enhanced their anti-fibrosis function, making them an effective therapeutic option for liver cirrhosis. In conclusion, our study demonstrated that Mi-BMSCs exhibited prolonged survival time *in vivo* and effectively ameliorated liver function, suppressed inflammation, and reduced fibrosis in both CCl_4-and TAA-induced liver cirrhosis models, primarily through the modulation of TGF-β/Smad signaling pathway. These findings highlight the potential of Mi-BMSCs as a promising therapeutic approach for early-stage liver cirrhosis. However, it is important to acknowledge some limitations of our study. Firstly, the evaluation of Mi-BMSCs in the context of cirrhosis with liver cancer was not conducted, and further investigations are warranted to assess their efficacy in cirrhosis and liver cancer treatment. Additionally, future studies should focus on validating these findings in large animal experiments to provide a more comprehensive understanding of the therapeutic potential of Mi-BMSCs and to further explore their vascular effects.

Funding

This work was Supported by Major scientific and technological innovation project of Wenzhou Science and Technology Bureau (Grant No. ZY2021009), Natural Science Foundation of Key Laboratory of Diagnosis and Treatment of Severe Hepato-Pancreatic Diseases of Zhejiang Province (No. G2023003), Shanghai Clinical Research Center for Interventional Medicine (NO.19MC1910300), the National Natural Science Foundation of China (Grant No.81972233), Discipline Cluster of Oncology, Wenzhou Medical University, China (NO. z2-2023015), Zhejiang Provincial Natural Science Foundation of China (LY24H160028), Wenzhou high-level innovation team (Development and application team of functional liver cancer-on-a-chip).

CRediT authorship contribution statement

Qing Shi: Writing – original draft, Visualization, Validation, Software, Methodology, Investigation, Formal analysis, Data curation, Conceptualization. **Yuhan Xia:** Writing – original draft, Visualization, Software, Methodology, Investigation. **Minmin Wu:** Visualization, Validation, Software, Methodology, Investigation, Data curation. **Yating Pan:** Methodology, Investigation. **Shiyi Wu:** Methodology. **Jiawei Lin:** Methodology. **Yifan Kong:** Methodology. **Zhijie Yu:** Supervision, Project administration. **Xingjie Zan:** Writing – review & editing, Supervision, Resources, Project administration, Funding acquisition, Conceptualization. **Pixu Liu:** Writing – review & editing, Supervision, Project administration. **Jinglin Xia:** Writing – review & editing, Supervision, Project administration, Funding acquisition, Conceptualization.

Declaration of competing interest

The authors declare that they have no known competing financial interests or personal relationships that could have appeared to influence the work reported in this paper.

Data availability

Data will be made available on request.

Acknowledgement

The authors would like to thank Xin Ma from Shiyanjia lab(www.shiyanjia.com) for Cryo-SEM service.

Appendix A. Supplementary data

Supplementary data to this article can be found online at https://doi.org/10.1016/j.mtbio.2024.100958.

References

[1] S.K. Asrani, H. Devarbhavi, J. Eaton, P.S. Kamath, Burden of liver diseases in the world, J. Hepatol. 70 (2019) 151–171, https://doi.org/10.1016/j.jhep.2018.09.014.
[2] A.H. Mokdad, et al., Global burden of diseases, injuries, and risk factors for young people's health during 1990-2013: a systematic analysis for the Global Burden of Disease Study 2013, Lancet 387 (2016) 2383–2401, https://doi.org/10.1016/S0140-6736(16)00648-6.
[3] T. Higashi, S.L. Friedman, Y. Hoshida, Hepatic stellate cells as key target in liver fibrosis, Adv. Drug Deliv. Rev. 121 (2017) 27–42, https://doi.org/10.1016/j.addr.2017.05.007.
[4] N.C. Henderson, F. Rieder, T.A. Wynn, Fibrosis: from mechanisms to medicines, Nature 587 (2020) 555–566, https://doi.org/10.1038/s41586-020-2938-9.

[5] C. Cicchini, et al., Molecular mechanisms controlling the phenotype and the EMT/MET dynamics of hepatocyte, Liver Int. 35 (2015) 302–310, https://doi.org/10.1111/liv.12577.
[6] F. Tacke, C. Trautwein, Mechanisms of liver fibrosis resolution, J. Hepatol. 63 (2015) 1038–1039, https://doi.org/10.1016/j.jhep.2015.03.039.
[7] L. Campana, H. Esser, M. Huch, S. Forbes, Liver regeneration and inflammation: from fundamental science to clinical applications, Nat. Rev. Mol. Cell Biol. 22 (2021) 608–624, https://doi.org/10.1038/s41580-021-00373-7.
[8] L. Chen, J. Qu, T. Cheng, X. Chen, C. Xiang, Menstrual blood-derived stem cells: toward therapeutic mechanisms, novel strategies, and future perspectives in the treatment of diseases, Stem Cell Res. Ther. 10 (2019) 406, https://doi.org/10.1186/s13287-019-1503-7.
[9] J. Galipeau, L. Sensebe, Mesenchymal stromal cells: clinical challenges and therapeutic opportunities, Cell Stem Cell 22 (2018) 824–833, https://doi.org/10.1016/j.stem.2018.05.004.
[10] European Association for the Study of the Liver, Electronic address, e. e. e. & European Association for the Study of the, L. EASL Clinical Practice Guidelines on prevention and management of bleeding and thrombosis in patients with cirrhosis, J. Hepatol. 76 (2022) 1151–1184, https://doi.org/10.1016/j.jhep.2021.09.003.
[11] T. Artzner, et al., Liver transplantation for critically ill cirrhotic patients: stratifying utility based on pretransplant factors, Am. J. Transplant. 20 (2020) 2437–2448, https://doi.org/10.1111/ajt.15852.
[12] M. Alfaifi, Y.W. Eom, P.N. Newsome, S.K. Baik, Mesenchymal stromal cell therapy for liver diseases, J. Hepatol. 68 (2018) 1272–1285, https://doi.org/10.1016/j.jhep.2018.01.030.
[13] M.M. Ni, et al., Novel Insights on Notch signaling pathways in liver fibrosis, Eur. J. Pharmacol. 826 (2018) 66–74, https://doi.org/10.1016/j.ejphar.2018.02.051.
[14] J.N. Wang, et al., Emerging role and therapeutic implication of Wnt signaling pathways in liver fibrosis, Gene 674 (2018) 57–69, https://doi.org/10.1016/j.gene.2018.06.053.
[15] K. Yoshida, et al., Clinico-pathological importance of TGF-beta/phospho-smad signaling during human hepatic fibrocarcinogenesis, Cancers 10 (2018), https://doi.org/10.3390/cancers10060183.
[16] J.H. Park, B. Park, K.K. Park, Suppression of hepatic epithelial-to-mesenchymal transition by melittin via blocking of TGFbeta/smad and MAPK-JNK signaling pathways, Toxins 9 (2017), https://doi.org/10.3390/toxins9040138.
[17] P. Liu, Y. Mao, Y. Xie, J. Wei, J. Yao, Stem cells for treatment of liver fibrosis/cirrhosis: clinical progress and therapeutic potential, Stem Cell Res. Ther. 13 (2022) 356, https://doi.org/10.1186/s13287-022-03041-5.
[18] D. Shi, et al., Quantitative evaluation of human bone mesenchymal stem cells rescuing fulminant hepatic failure in pigs, Gut 66 (2017) 955–964, https://doi.org/10.1136/gutjnl-2015-311146.
[19] J. Han, C. Lee, J. Hur, Y. Jung, Current therapeutic options and potential of mesenchymal stem cell therapy for alcoholic liver disease, Cells 12 (2022), https://doi.org/10.3390/cells12010022.
[20] T. Zhou, et al., Challenges and advances in clinical applications of mesenchymal stromal cells, J. Hematol. Oncol. 14 (2021) 24, https://doi.org/10.1186/s13045-021-01037-x.
[21] M. Shi, et al., Mesenchymal stem cell therapy in decompensated liver cirrhosis: a long-term follow-up analysis of the randomized controlled clinical trial, Hepatol Int 15 (2021) 1431–1441, https://doi.org/10.1007/s12072-021-10199-2.
[22] M. Yuan, X. Hu, L. Yao, Y. Jiang, L. Li, Mesenchymal stem cell homing to improve therapeutic efficacy in liver disease, Stem Cell Res. Ther. 13 (2022) 179, https://doi.org/10.1186/s13287-022-02858-4.
[23] A. Tsuchiya, et al., Mesenchymal stem cell therapies for liver cirrhosis: MSCs as "conducting cells" for improvement of liver fibrosis and regeneration, Inflamm. Regen. 39 (2019) 18, https://doi.org/10.1186/s41232-019-0107-z.
[24] T. Song, H. Zhang, Z. Luo, L. Shang, Y. Zhao, Primary human pancreatic cancer cells cultivation in microfluidic hydrogel microcapsules for drug evaluation, Adv. Sci. 10 (2023) e2206004, https://doi.org/10.1002/advs.202206004.
[25] R.D. Levit, N. Landázuri, E.A. Phelps, M.E. Brown, A.J. García, M.E. Davis, G. Joseph, R. Long, S.A. Safley, J.D. Suever, A.N. Lyle, C.J. Weber, W.R. Taylor, Cellular encapsulation enhances cardiac repair, J. Am. Heart Assoc. 2 (5) (2013 Oct 10) e000367, https://doi.org/10.1161/JAHA.113.000367.
[26] A. Maged, R. Abdelbaset, A.A. Mahmoud, N.A. Elkasabgy, Merits and advances of microfluidics in the pharmaceutical field: design technologies and future prospects, Drug Deliv. 29 (2022) 1549–1570, https://doi.org/10.1080/10717544.2022.2069878.
[27] B. Li, et al., Droplets microfluidics platform-A tool for single cell research, Front. Bioeng. Biotechnol. 11 (2023) 1121870, https://doi.org/10.3389/fbioe.2023.1121870.
[28] C. Shao, J. Chi, L. Shang, Q. Fan, F. Ye, Droplet microfluidics-based biomedical microcarriers, Acta Biomater. 138 (2022) 21–33, https://doi.org/10.1016/j.actbio.2021.10.037.
[29] H. Zhu, et al., A protocol for isolation and culture of mesenchymal stem cells from mouse compact bone, Nat. Protoc. 5 (2010) 550–560, https://doi.org/10.1038/nprot.2009.238.
[30] Y. Popov, et al., Tissue transglutaminase does not affect fibrotic matrix stability or regression of liver fibrosis in mice, Gastroenterology 140 (2011) 1642–1652, https://doi.org/10.1053/j.gastro.2011.01.040.
[31] J. Li, et al., Magnetic resonance diffusion kurtosis imaging for evaluating stage of liver fibrosis in a rabbit model, Acad. Radiol. 26 (2019) e90–e97, https://doi.org/10.1016/j.acra.2018.06.018.
[32] X. Rong, et al., Human bone marrow mesenchymal stem cells-derived exosomes alleviate liver fibrosis through the Wnt/beta-catenin pathway, Stem Cell Res. Ther. 10 (2019) 98, https://doi.org/10.1186/s13287-019-1204-2.
[33] Y. Feng, et al., Bone marrow mesenchymal stem cells inhibit hepatic fibrosis via the AABR07028795.2/rno-miR-667-5p axis, Stem Cell Res. Ther. 13 (2022) 375, https://doi.org/10.1186/s13287-022-03069-7.
[34] E. El Agha, et al., Mesenchymal stem cells in fibrotic disease, Cell Stem Cell 21 (2017) 166–177, https://doi.org/10.1016/j.stem.2017.07.011.
[35] F. Zheng, Y. Xiao, H. Liu, Y. Fan, M. Dao, Patient-specific organoid and organ-on-a-chip: 3D cell-culture meets 3D printing and numerical simulation, Adv Biol (Weinh) 5 (2021) e2000024, https://doi.org/10.1002/adbi.202000024.
[36] S. Shrestha, V.K.R. Lekkala, P. Acharya, D. Siddhpura, M.Y. Lee, Recent advances in microarray 3D bioprinting for high-throughput spheroid and tissue culture and analysis, Essays Biochem. 65 (2021) 481–489, https://doi.org/10.1042/EBC20200150.
[37] G. Chiabotto, E. Ceccotti, M. Tapparo, G. Camussi, S. Bruno, Human liver stem cell-derived extracellular vesicles target hepatic stellate cells and attenuate their pro-fibrotic phenotype, Front. Cell Dev. Biol. 9 (2021) 777462, https://doi.org/10.3389/fcell.2021.777462.
[38] J.S. Rockel, R. Rabani, S. Viswanathan, Anti-fibrotic mechanisms of exogenously-expanded mesenchymal stromal cells for fibrotic diseases, Semin. Cell Dev. Biol. 101 (2020) 87–103, https://doi.org/10.1016/j.semcdb.2019.10.014.
[39] K.Y. Lee, D.J. Mooney, Alginate: properties and biomedical applications, Prog. Polym. Sci. 37 (1) (2012) 106–126, https://doi.org/10.1016/j.progpolymsci.2011.06.003.
[40] T. Tsuchida, S.L. Friedman, Mechanisms of hepatic stellate cell activation, Nat. Rev. Gastroenterol. Hepatol. 14 (2017) 397–411, https://doi.org/10.1038/nrgastro.2017.38.
[41] S.K. Hamilton, N.C. Bloodworth, C.S. Massad, T.M. Hammoudi, S. Suri, P.J. Yang, et al., Development of 3D hydrogel culture systems with on-demand cell separation, Biotechnol. J. 8 (4) (2013) 485–495.
[42] X. Zhao, S. Liu, L. Yildirimer, H. Zhao, R.H. Ding, H.N. Wang, et al., Injectable stem cell-laden photocrosslinkable microspheres fabricated using microfluidics for rapid generation of osteogenic tissue constructs, Adv. Funct. Mater. 26 (17) (2016) 2809–2819, https://doi.org/10.1002/biot.201200200.
[43] G.F. Gao, A.F. Schilling, K. Hubbell, T. Yonezawa, D. Truong, Y. Hong, et al., Improved properties of bone and cartilage tissue from 3D inkjet-bioprinted human mesenchymal stem cells by simultaneous deposition and photocrosslinking in PEG-GelMA, Biotechnol. Lett. 37 (11) (2015) 2349–2355, https://doi.org/10.1007/s10529-015-1921-2.